AGU PUBLICATIONS

Geochemistry, Geophysics, Geosystems

RESEARCH ARTICLE
10.1002/2017GC006988

Special Section:
Magnetism From Atomic to Planetary Scales: Physical Principles and Interdisciplinary Applications in Geo- and Planetary Sciences

Early diagenetic greigite as an indicator of paleosalinity changes in the middle Miocene Paratethys Sea of central Europe

Suzhen Liu[1,2], Wout Krijgsman[1], Mark J. Dekkers[1], and Dan Palcu[1]

[1]Paleomagnetic Laboratory "Fort Hoofddijk", Department of Earth Sciences, Utrecht University, Utrecht, The Netherlands, [2]State Key Laboratory of Lithospheric Evolution, Institute of Geology and Geophysics, Chinese Academy of Sciences, Beijing, China

Key Points:
- Four greigite-bearing layers are identified in the Tisa section (Romania) after the Badenian-Sarmatian Extinction Event at 12.65 Ma
- Greigite formation is associated with a decreased salinity due to fresh water infill into the Central Paratethys from the Eastern Paratethys
- The greigite layers are tentatively correlated to eccentricity maxima suggesting a possible Milankovitch forcing of the gateway functioning

Supporting Information:
- Supporting Information S1

Correspondence to:
S. Liu,
s.liu@uu.nl

Citation:
Liu, S., W. Krijgsman, M. J. Dekkers, and D. Palcu (2017), Early diagenetic greigite as an indicator of paleosalinity changes in the middle Miocene Paratethys Sea of central Europe, *Geochem. Geophys. Geosyst.*, *18*, 2634–2645, doi:10.1002/2017GC006988.

Received 27 APR 2017
Accepted 16 JUN 2017
Accepted article online 1 JUL 2017
Published online 22 JUL 2017

Abstract The Miocene epicontinental Paratethys Sea of central Eurasia has experienced multiple restriction and reconnection events to the open ocean. Magnetostratigraphy is an important dating tool to better understand the temporal and spatial paleoenvironmental variations associated with these changes. Magnetostratigraphy in the Paratethys domain, however, is complicated by the presence of greigite (Fe_3S_4). Here we report rock magnetic and X-ray fluorescence data of the Tisa section (Romania) which was previously magnetostratigraphically dated at the middle Miocene (base at 12.8 Ma and top at 12.2 Ma). This section comprises the Badenian Sarmatian Extinction Event (BSEE), which is marked by a major salinity change from marine to brackish environments, related to the opening of the connection between the Central and the Eastern Paratethys basins. In the marine Badenian sediments below the BSEE, the pyritization process is shown to be complete because of abundant sulfate supply. In the brackish Sarmatian deposits, four intervals with early diagenetic greigite are observed, and linked to insufficient sulfate in the water column. These four greigite intervals appear to correspond to maxima in the ~100 kyr eccentricity cycle. We propose that increased fresh water from the Eastern Paratethys basin during eccentricity maxima restricted the sulfate availability in the Tisa area, leading to a reduced HS^- production and enhanced greigite preservation. The early diagenetic formation of greigite enables a quasi syn-depositional recording of the paleomagnetic field, which allows reliable paleomagnetic dating in this section. Our results further suggest greigite as a potential indicator for salinity changes during marine/brackish transitions.

1. Introduction

The Paratethys Sea is the large epicontinental sea of central Eurasia that originated in Eocene-Oligocene times from the collision of the Indian and Arabian plates with Eurasia [*Laskarev*, 1924; *Rögl*, 1999; *Schulz et al*., 2005]. With its extension from central Europe to western China, the Paratethys represents an ideal natural laboratory to explore links between sea-land distribution, climate change, and biological migration [e.g., *Harzhauser and Piller*, 2007; *Karami et al*., 2011; *Ramstein et al*., 1997]. Orogenic processes in the Alpine-Himalayan mountain belt combined with global eustatic sea-level changes repeatedly restricted, isolated, and reconnected, the various Paratethyan subbasins from and to the open ocean, resulting in extreme paleoenvironmental changes from hypersaline and anoxic to brackish and fresh water conditions. The Paratethys is divided into three paleogeographic units, named Western, Central, and Eastern Paratethys. The Central Paratethys was located in the present central Europe, while the Eastern Paratethys covered the region of present-day Black Sea, Caspian Sea, and Aral Sea.

The dominantly endemic faunal assemblages and the scarcity of volcanic ash layers suitable for radioisotopic dating hamper the construction of robust time frames for the Paratethyan basins. Precise correlation to the global geological time scale is therefore not straightforward. Magnetostratigraphy could be a suitable dating technique, but the common presence of the magnetic iron sulphide greigite (Fe_3S_4) in the Paratethys complicates the interpretation of the paleomagnetic records [e.g., *Hsü and Giovanoli*, 1979; *Król and Jeleńska*, 1999; *Babinszki et al*., 2007; *Sant et al*., 2015]. Previous studies have shown that late diagenetic greigite with its inherent remagnetization can originate from multiple mechanisms [*Roberts and Weaver*, 2005]. This may involve various geological processes such as percolation of oxic fluids and/or sea-level changes [*Jiang et al*., 2001;

Oda and Torii, 2004; *Rowan and Roberts*, 2006; *Sagnotti et al*., 2010]. However, high-resolution magnetostratigraphic studies on the late Miocene sedimentary successions in Romania [*Vasiliev et al*., 2004, 2005] and in the Black Sea basin [*Krijgsman et al*., 2010; *Chang et al*., 2014; *van Baak et al*., 2016] resulted in straightforward correlations to the Geomagnetic Polarity Time Scale (GPTS) and confirm the reliability of these greigite-based magnetostratigraphic time frames. In these sections, the magnetic signal is carried by biogenic greigite of primary origin (generated intracellularly by magnetotactic bacteria) and/or authigenic greigite of secondary origin that formed by early diagenetic processes [*Vasiliev et al*., 2007, 2008]. Therefore, assessment of the greigite formation mechanism on a case-by-case basis is necessary for robust magnetostratigraphic dating in the Paratethys region [e.g., *Aben et al*., 2014].

Since organic matter and sulfate availability are indispensable for greigite production, the occurrence of greigite in geological records was used to reflect variations in organic matter [e.g., *Blanchet et al*., 2009] and salinity changes [*Reynolds et al*., 1998; *Reynolds and Rosenbaum*, 2005]. Greigite preservation in the Paratethys sediments has also been shown to be environmentally/climatically controlled by cyclostratigraphic correlation to astronomical curves. In their study of the Miocene Black Sea sediments, *Chang et al*. [2014] linked the diagenetic greigite formation in brackish environments to variations in terrigenous input, while in fresh water to the variations in the concentration of dissolved pore water sulfate. These results demonstrate the potential of greigite as an indicator to better understand paleoenvironmental changes.

The Badenian-Sarmatian Extinction Event (BSEE) is one of the most dramatic paleoenvironmental changes in central Europe, with 588 last occurrences of gastropods species and 121 last occurrences of foraminifera species [*Harzhauser and Piller*, 2007]. The Badenian and Sarmatian are regional stage names in the Paratethys realm. The Badenian refers to a stage equivalent to the late Langhian and early Seravallian while the Sarmatian refers to a stage during the late Seravallian. The BSEE is assumed to have been triggered by the activation of the gateway between the Central Paratethys and the Eastern Paratethys Basin (Figure 1), generating a sudden transition from open marine to brackish conditions in the Central Paratethys [*Palcu et al*., 2015]. The only robust magnetostratigraphic BSEE record is from the Tisa section in Romania, which dates the event at 12.65 Ma [*Palcu et al*., 2015]. Other sections that contain the BSEE have paleomagnetic signals that are difficult to interpret due to the presence of multiple magnetic components [*de Leeuw et al*., 2013]

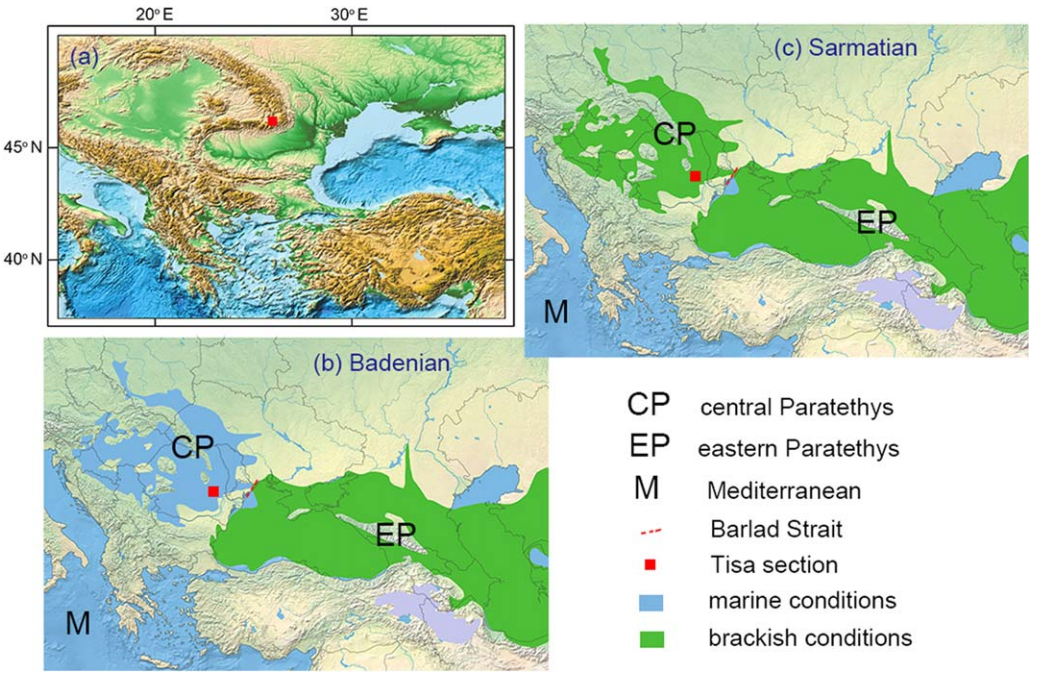

Figure 1. Geological background of the study site. (a) Location of the Tisa section (red square) shown together with the Black Sea, the Mediterranean, and the Carpathian Foredeep. Figures 1b and 1c are paleogeographic maps before and after the Badenian-Sarmatian Extinction Event. The Central Paratethys Basin where the Tisa section is located, changes from an open marine setting in the Badenian to a brackish setting in the Sarmatian by water influx through the Barlad Strait [*Palcu et al*., 2015]. The Eastern Paratethys Basin remains in brackish conditions throughout this period because it contains a much larger water volume than its central counterpart.

or late diagenetic greigite components [*Sant et al*., 2015]. The paleomagnetic signal of the interval straddling the BSEE in the Tisa section shows a mixture of samples dominated by magnetite and/or greigite [*Palcu et al*., 2015].

In this study, we perform a combined environmental magnetic and X-ray fluorescence (XRF) study on the Badenian and Sarmatian sediments of the Tisa section (~12.79 to ~12.20 Ma) of the Carpathian Foredeep. By identifying the magnetic mineral formation mechanism, we aim to clarify the changes in redox conditions and sulfate concentrations across the BSEE. Moreover, our results are tentatively correlated with orbital parameters suggesting a possible climatic and hydrologic driver on the magnetic mineral variations in the Tisa section.

2. Geological Setting, Sampling, and Chronology

The Tisa section (45°17.565′N, 26°29.567′E) is located in southeastern Romania, in the vicinity of the bend area of the Carpathian Mountains. During the middle Miocene, it was located in the southeastern part of the Carpathian Foredeep Basin, in the vicinity of the Barlad Strait—the gateway linking the Central Paratethys with the Eastern Paratehtys (Figure 1). The proximity of the gateway makes it an appropriate section to study the connectivity changes responsible for the BSEE.

The lower part (Badenian) of the Tisa section (Figure 2a) mainly comprises gray marls interbedded in sandstones. The middle part, including the BSEE, consists of essentially homogenous marls with occasional sandy laminae. The upper part (Sarmatian) shows an irregular alternation of gray marls and sandstones, while homogeneous gray marls dominate the top of the succession again.

A collection of oriented samples (labeled TS) was drilled in 98 stratigraphic levels in the Tisa section in 2012, which cover 223 m stratigraphy. For a more detailed research of the Badenian-Sarmatian boundary, another 128 samples (labeled VT) were taken in higher resolution between 39 and 91 m in 2014. The age framework of the Tisa section is based on magnetostratigraphic dating combined with high-resolution biostratigraphy on calcareous nannofossils and foraminifera [*Palcu et al*., 2015]. Correlation of the polarity pattern to the GPTS yields four tie points corresponding to the normal polarity chron boundaries of C5Ar.1n and C5An.2n (at 12.272, 12.474, 12.735, and 12.77 Ma). By extrapolation, the base and top of the section were put at 12.79 and 12.21 Ma, respectively. The Badenian-Sarmatian boundary is located at ~68 m and has an interpolated age of 12.65 ± 0.01 Ma. Fauna analyses in Tisa section indicate a major shift from marine to brackish water conditions coinciding with the Badenian-Sarmatian boundary [*Palcu et al*., 2015].

3. Methods

Room temperature hysteresis loops, back-field demagnetization of saturated isothermal remanent magnetization (SIRM) were measured with a Princeton Measurements Corporation MicroMag 2900 alternating gradient magnetometer (AGM, noise level 2×10^{-9} Am^2). Hysteresis loops (sample mass 60–90 mg) were acquired between −1 and 1 T with a field increment of 10 mT. The saturation magnetization (M_s), the saturation remanent magnetization (M_{rs}), and coercivity (B_c) were acquired after correction for the paramagnetic slope (at 70% of the maximum field). Back field demagnetization of SIRM was performed after saturating the sample in a field of 1 T to determine the remanence coercivity (B_{cr}). For first-order reversal curves (FORCs), 150 reversal curves were obtained for each sample with a field increment of 1.5 mT. FORC diagrams were calculated using the FORCme software package [*Heslop and Roberts*, 2012]. All the measurements on AGM were performed with an averaging time of 500 ms.

High-temperature thermomagnetic measurements of the induced magnetization (*J-T* curves) were performed in air with a modified horizontal translation-type Curie balance with a sensitivity of $\sim 5 \times 10^{-9}$ Am^2 [*Mullender et al*., 1993]. About 100 mg powdered sediments were held in place by quartz wool in a quartz glass holder. The applied field was cycled between 100 and 300 mT or between 150 and 300 mT depending on the intensity of the magnetization. Multiple heating and cooling runs were performed between room temperature, 150, 250 350, 450, 500, and 700°C. The heating rate was 6°C/min and the cooling rate was 10°C/min.

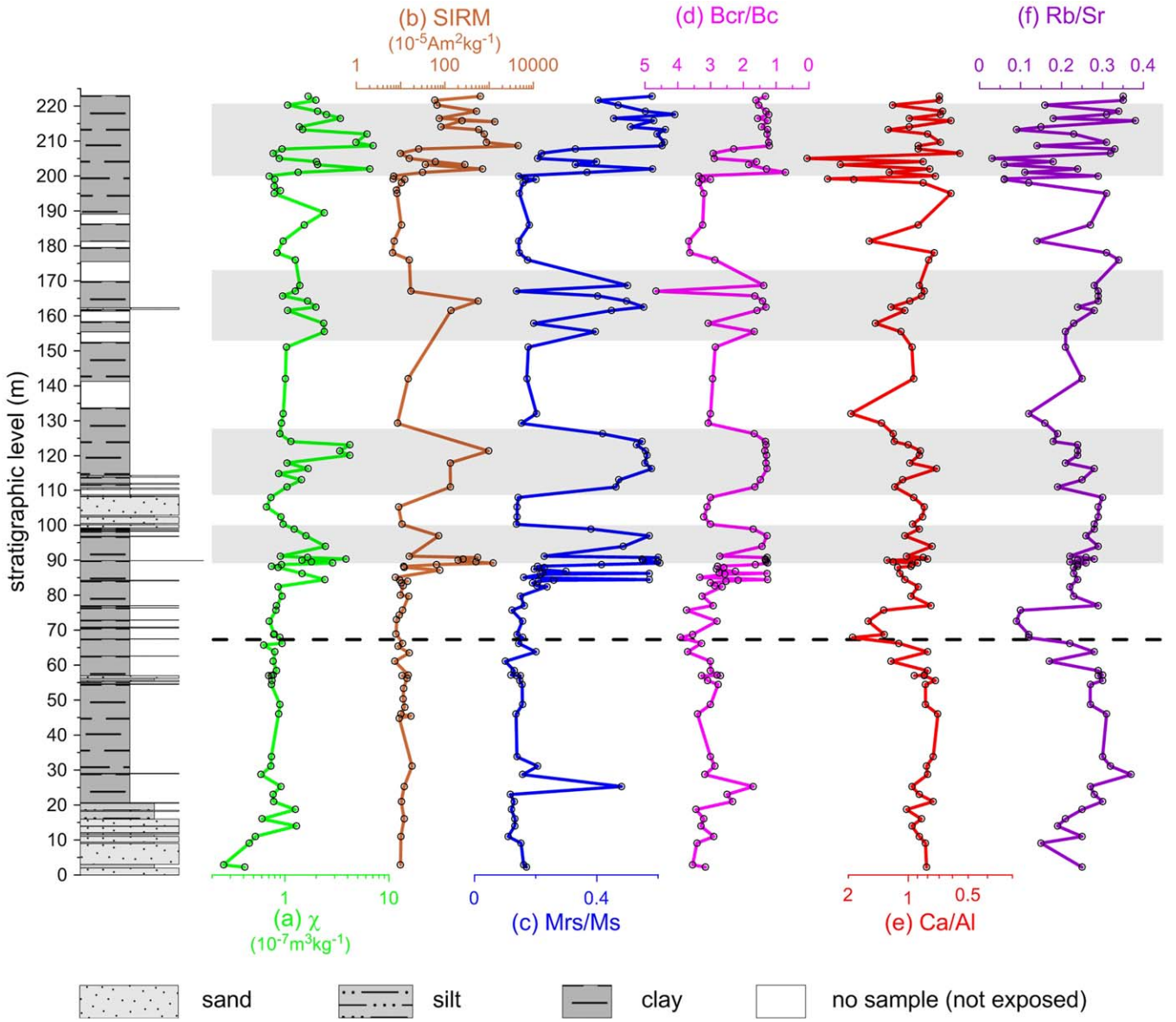

Figure 2. Stratigraphic variations in the magnetic and geochemical parameters of the Tisa section. (a) Lithology of the Tisa section. Figures 2b and 2c are mass normalized magnetic susceptibility (χ) and mass normalized saturation isothermal remanent magnetization (SIRM), respectively. The magnetic susceptibility data are from *Palcu et al.* [2015]. (d) Ratio of remanent saturation magnetization (M_{rs}) to saturation magnetization (M_s). (e) Ratio of remanence coercivity (B_{cr}) to coercivity (B_c). Figures 2f and 2g are ratios of elemental concentration from X-ray fluorescence (XRF). The dashed line represents the Badenian-Sarmatian boundary. The gray bars denote intervals with early diagenetic greigite.

In addition, elemental changes were analyzed using a handheld Thermo Scientific Niton XL3t XRF Analyzer. Measurements were performed in the so-called Mining mode (Cu/Zn) under a steady flow of helium gas. Samples were measured after a flat fresh surface was cut by a plastic knife on the cored samples. A standard sample was repeatedly measured between every 10 measurements to check the reproducibility. The data are semiquantitative suited to track the elemental trends through the sequence rather than the absolute elemental concentrations.

4. Results

4.1. Stratigraphic Trends in Magnetic and Geochemical Parameters

Figure 2 shows variations of magnetic parameters (Figures 2b–2e) and XRF data (Figures 2f–2g, original XRF data with error bars are shown in supporting information Figure S1). Consistent variations in χ and SIRM

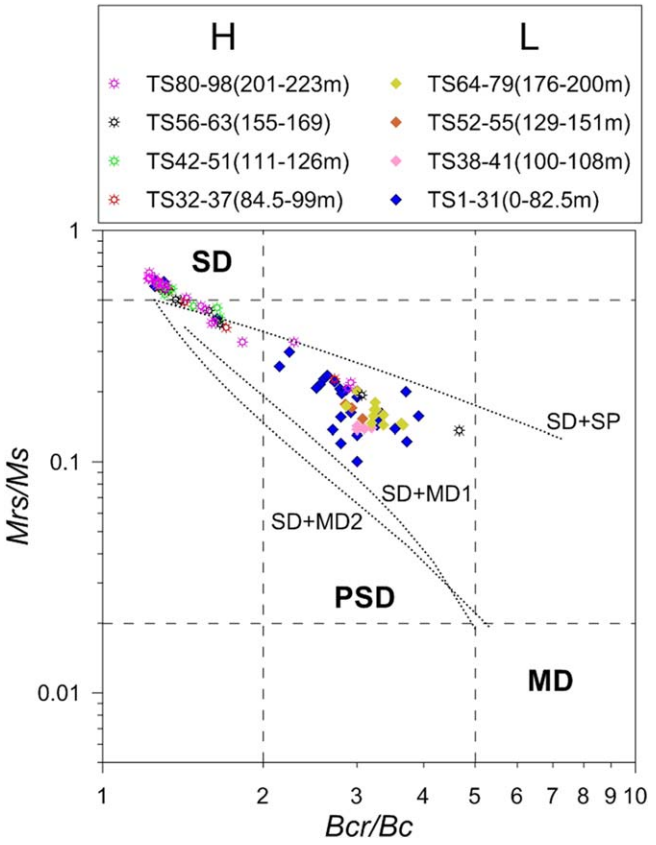

Figure 3. Magnetic hysteresis parameters on a Day plot [*Day et al.*, 1977]. The magnetite single domain (SD), pseudo-single-domain (PSD), and multidomain (MD) grains areas are indicated by the dashed lines, and mixing lines for SD + SP (superparamagnetic), SD + MD1, SD + MD2 particles are shown by dotted lines, according to *Dunlop* [2002]. H stands for the high magnetic samples in the Sarmatian, which almost all cluster in or near the SD area. L stands for low magnetic samples in the Sarmatian and all Badenian samples.

indicate that the low and high magnetic fluctuations are controlled by magnetic concentration rather than magnetic grain size.

We divide the magnetic data into two groups: The low magnetic samples have χ of less than 10^{-7} m^3 kg^{-1} [*Palcu et al.*, 2015] and SIRM around 10^{-4} Am^2 kg^{-1}, which is low for sediments. These samples have low ratios of M_{rs}/M_s (<0.2) and corresponding high ratios of B_{cr}/B_c (>2.8). They almost all fall in the pseudo-single domain (PSD) area of the Day Plot (Figure 3, original hysteresis parameters can be found in supporting information Table S1) [*Day et al.*, 1977; *Dunlop*, 2002]. The high magnetic samples have high ratios of M_{rs}/M_s (>0.2, mostly >0.4) and corresponding low ratios of B_{cr}/B_c (<2.8). On the Day plot, they cluster in or near the SD area following the SD + SP mixing line. The Badenian (0–68 m) is dominated by low magnetic samples. In the Sarmatian (68–220 m), four low magnetic and four high magnetic units occur alternately.

Stratigraphic elemental variations, represented by the ratio of Ca to Al and that of Rb to Sr, are plotted with ratios of magnetic parameters for the high (Figures 4a–4d) and low (Figures 4e–4h) magnetic units, respectively. Assuming that sedimentary Al is contained in silicates of detrital origin and Ca comes from biogenic calcium carbonate, the Ca/Al ratio represents the contribution of carbonate production in the ocean over terrigenous input [e.g., *Jaccard et al.*, 2005]. Similarly, given that Sr can be leached much easier than Rb, a higher Rb/Sr ratio implies more weathered terrigenous detritus [e.g., *Chen et al.*, 1999]. Their anti-phase variation (Figures 2f–2g) testifies to the robustness of these two ratios. Despite the fluctuations in both ratios, however, barely any correlation is found between the elemental changes and the magnetic parameters. The coefficient of determination (R^2) is smaller than 0.091 for the low magnetic units and smaller than 0.124 for the high magnetic units (Figure 4).

4.2. Magnetic Properties of Representative Samples

Representative samples from the low and high magnetic units show distinctive magnetic properties in both room temperature (Figure 5) and high-temperature measurements (Figure 6). Samples from the high magnetic units have open hysteresis loops, with coercivity and remanence coercivity as high as ~45 and ~60 mT, respectively. Their FORC distribution is similar to those previously reported for SD diagenetic greigite [*Roberts et al.*, 2011, 2006]. The diagrams have classic SD-like contours centered on $B_c \sim 60$ mT. Considerable magnetic interaction is indicated by the large vertical spread. The central peak is not symmetrical with respect to the B_u axis but shifted to the negative area below $B_u = 0$. For the *J-T* curves, all the high magnetic samples show an irreversible decrease in magnetization between 200°C and 350°C, which is typical of greigite [e.g., *Dekkers et al.*, 2000]. Pyrite also exists in these samples, indicated by the magnetization increase after 400°C (due to its oxidation via magnetite ultimately to hematite) [*Passier et al.*, 2001].

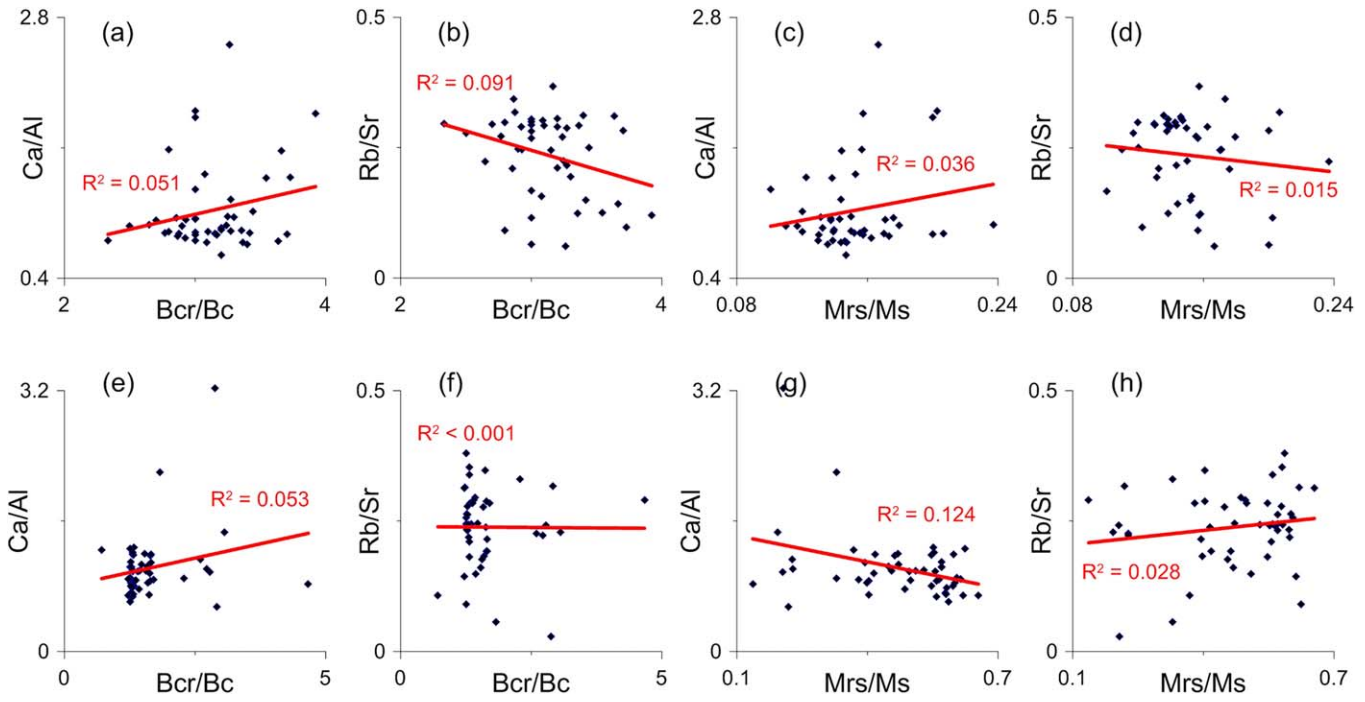

Figure 4. Correlation between different magnetic and elemental variations for the (a–d) low magnetic samples and (e–h) high magnetic samples, respectively. The red lines are fit on the premise of a linear correlation. The low coefficients of determinations (R^2) point to the absence of a significant correlation between the magnetic properties (alternation of greigite and pyrite in the sediments) and variations in Ca/Al ratios (indicative of biogenic production in the ocean) and Rb/Sr (terrigenous input from the continent).

On the other hand, the low magnetic samples are dominated by paramagnetic minerals, suggested by the essentially linear magnetization curve before paramagnetic correction. After correction, the samples show a low coercivity below 10 mT and, correspondingly, a low remanence coercivity of ~30 mT. Due to its low

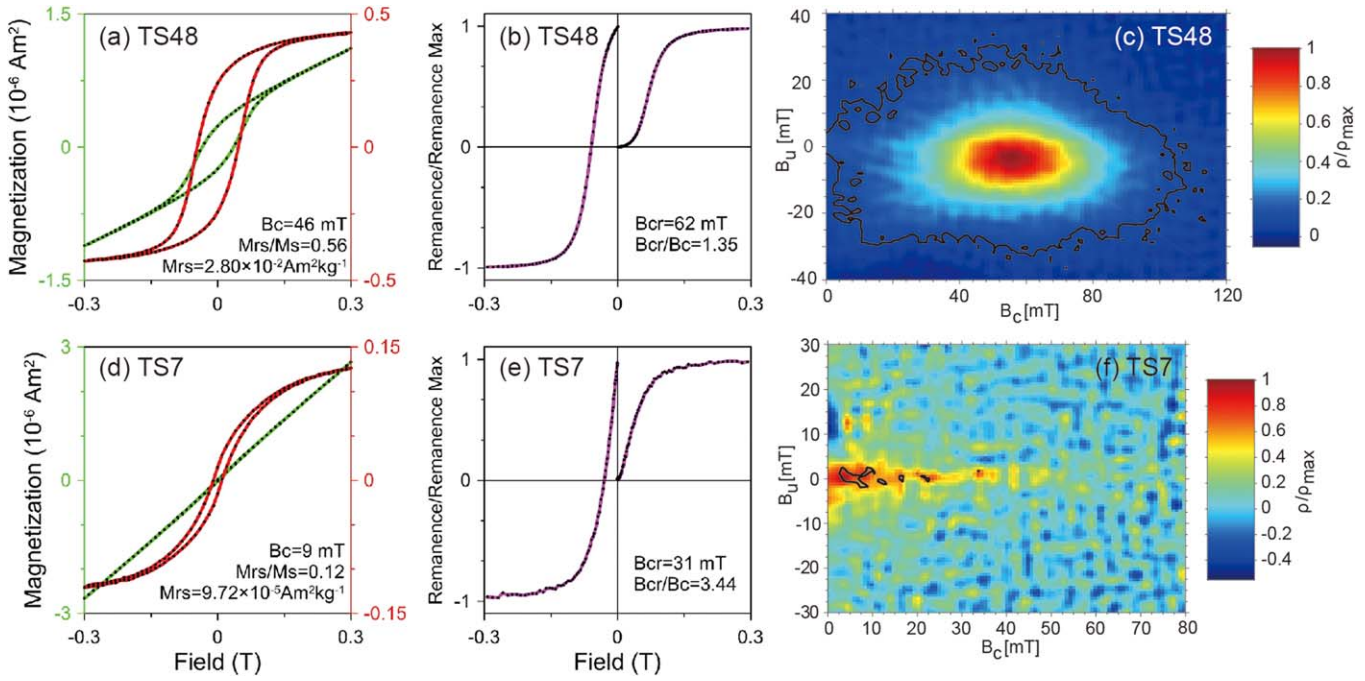

Figure 5. Rock magnetic results of two representative samples. TS48 is from the high magnetic units and TS7 from the low magnetic units. (a) and (d) Blow ups of the central portions of hysteresis loops (measured to a maximum field of ±1 T). The green lines and red lines indicate results before and after paramagnetic corrections, respectively. (b) and (e) IRM acquisition and back field demagnetization curves; central portions of ±0.3 T for clear view. Samples were measured up to 1 T. (c) and (f) First-order reversal curve (FORC) diagrams were generated with smoothing factor (SF) of 3. Black line in Figures 5c and 5f indicates 95% confidence level [*Heslop and Roberts*, 2012].

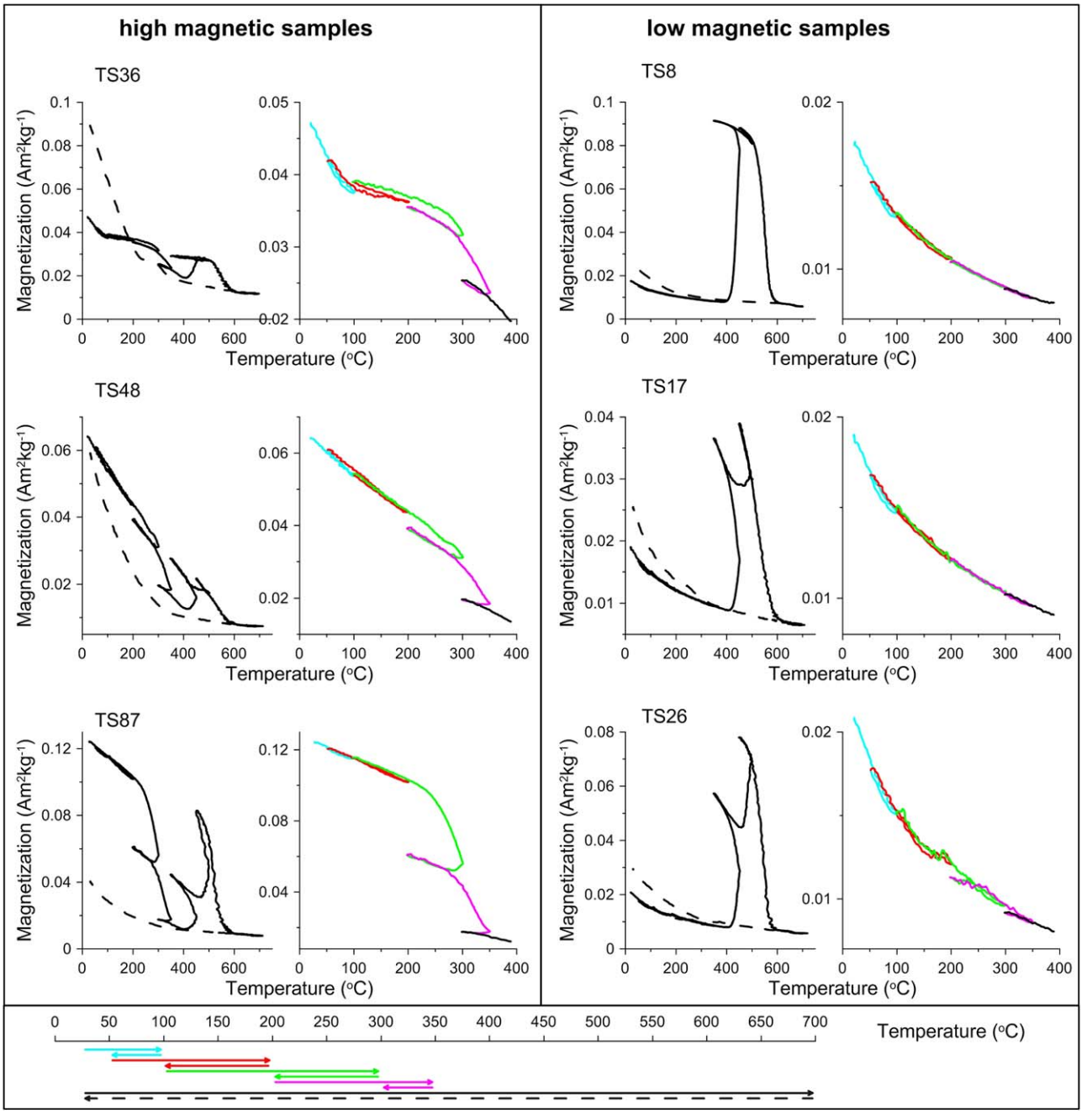

Figure 6. Dependence of magnetization on temperature during repeated thermal runs on Curie Balance. The low and high magnetic samples show distinct behavior. For each sample, the plot on the left shows results of the whole heating and cooling process, and the plot on the right is an enlarged view of variations below 400°C. Legends for the temperature intervals are shown at the bottom. The irreversible decreases in magnetization between 200°C and 350°C are typical for greigite [e.g., *Dekkers et al*., 2000]. Magnetization increases after 400°C are likely due to oxidation of pyrite to magnetite [*Passier et al*., 2001].

intensity (two orders of magnitude lower than the high magnetic samples), only a weak FORC distribution is observable, centered on $B_c < 10$ mT. This may origin from a very low amount of magnetite (supporting information Figure S2), which is also responsible for the hysteresis and the weak NRM. The low amount of magnetite in diagenetic sediments is probably residing in inclusions in silicate hosts [*Chang et al*., 2016]. The *J-T* curves of these low magnetic samples are reversible during thermal runs below 400°C. The large increases after 400°C indicate large amounts of pyrite in these samples which oxidize to magnetite causing the peak at 450–500°C in *J-T* curves. Abundant pyrite in these samples is also consistent with the low intensity and subtle hysteresis since pyrite is paramagnetic.

5. Discussion

5.1. Mechanism for Greigite Formation

Iron sulfides like greigite and pyrite form in reducing sedimentary environments. Major factors that control iron sulfide production (actually the supply of Fe^{2+} and HS^-) are the amount of organic matter, the amount and reactivity of iron-bearing minerals in the sediments, and the availability of dissolved sulfate [*Berner*, 1984]. Since it takes twice the amount of elemental sulfur to convert greigite (Fe_3S_4) into pyrite (FeS_2) than to form greigite from mackinawite (FeS) [*Fu et al*., 2008], in case of a surplus of Fe^{2+} over HS^- pyritization process will be arrested and greigite as an intermediate will be preserved [*Kao et al*., 2004]. *Blanchet et al*. [2009] invoked the availability of organic matter as the controlling factor of greigite preservation in Santa Barbara Basin (California, USA), based on the correlation of greigite-enriched layers with low organic matter content. A similar mechanism was proposed in the Miocene Black Sea where greigite was preserved in organic-poor sedimentary layers with high terrigenous input [*Chang et al*., 2014]. On the contrary, for the same section when the depositional environment switched from a marine to a lake setting, dissolved sulfate concentration and biogenic productivity was identified as the limiting factor that results in the formation of greigite rather than pyrite [*Chang et al*., 2014].

In the Tisa section, the greigite layers correlate neither with high continental input (represented by high ratios of Rb to Sr) nor with high biogenic production (represented by high ratios of Ca to Al). Therefore, we exclude organic matter as the predominant controlling factor for greigite formation. The absence of greigite in the marine Badenian and its preservation in the brackish Sarmatian sediments implies a salinity influence on the magnetic mineralogy. According to *Berner* [1984, references therein], bacterial sulfate reduction is efficient enough to provide abundant HS^- in marine settings where sulfate concentrations are high. Fresh waters generally have a lower sulfate content which could lead to greigite preservation. The hypothesis that greigite represents increased freshness in the otherwise saline water column was proposed by *Reynolds et al*. [1998] in their study of Owens Lake (California, USA). An analogy to this salinity-related greigite formation hypothesis was also reported by *Reynolds and Rosenbaum* [2005] in the Bear Lake watershed (Utah, Idaho and Wyoming, USA).

During the Badenian, the local paleoenvironmental conditions in the Tisa section are fully marine, because of an open connection with the Mediterranean [*Palcu et al*., 2015]. Therefore, the abundance of HS^- leads to full pyritization and no greigite is preserved in the Badenian (Figure 7a). After the Badenian-Sarmatian transition at ~12.65 Ma, the newly activated Barlad Gateway gradually connects the Central Paratethys with the brackish water domain of the Eastern Paratethys basin (Figure 1). Fauna analyses in Tisa section indicate a major shift from marine to brackish water conditions coinciding with the Badenian-Sarmatian boundary [*Palcu et al*., 2015]. We therefore attribute the greigite occurrences in the Sarmatian deposits of the Tisa section to insufficient sulfate supply due to enhanced freshwater input from the Eastern Paratethys basin, which significantly reduced the salinity in the Central Paratethys (Figure 7b).

5.2. Correlation of Greigite Layers with Eccentricity Maxima: Tentative Orbital Forcing

The age model of the greigite-bearing layers in the Tisa section was constructed by linear interpolation of paleomagnetic polarity tie points. The greigite layers in the Sarmatian occur at 12.24, 12.36, 12.47, and 12.57 Ma suggesting a linkage, within error, to the eccentricity maxima in the LA04 insolation curve [*Laskar et al*., 2004] (Figure 8). We thus propose a tentative 100 kyr eccentricity forcing of the greigite formation in Tisa.

The 100 kyr eccentricity cycles have been often reported to dominate late Pleistocene climate records [e.g., *Hays et al*., 1976; *Raymo*, 1994; *Kukla et al*., 1988]. Since the changes in total received insolation due to changes in eccentricity can vary by no more than 0.2% around the long-term mean [*Ruddiman*, 2014], it is difficult to explain this periodicity in terms of a direct response to the eccentricity forcing. *Imbrie et al*. [1993] ascribed this periodicity to the large northern hemisphere ice sheets and to the coupled air-sea-ice system as a nonlinear amplifier. These 100 kyr eccentricity cycles have also been recovered during the Miocene before the formation of northern Hemisphere ice sheets. Fluctuations of the Antarctic ice sheets instead of their northern hemisphere counterparts were proposed as a linkage [*Beaufort*, 1994; *Nie et al*., 2017].

The 100 kyr cycles in the Tisa section may also origin from eccentricity-driven sea-ice relation. During the eccentricity maxima, shrinking Antarctic ice sheets release water into the ocean. The ensuing high sea level enhances the exchange through the Barlad Gateway, which brings additional fresh water from the Eastern

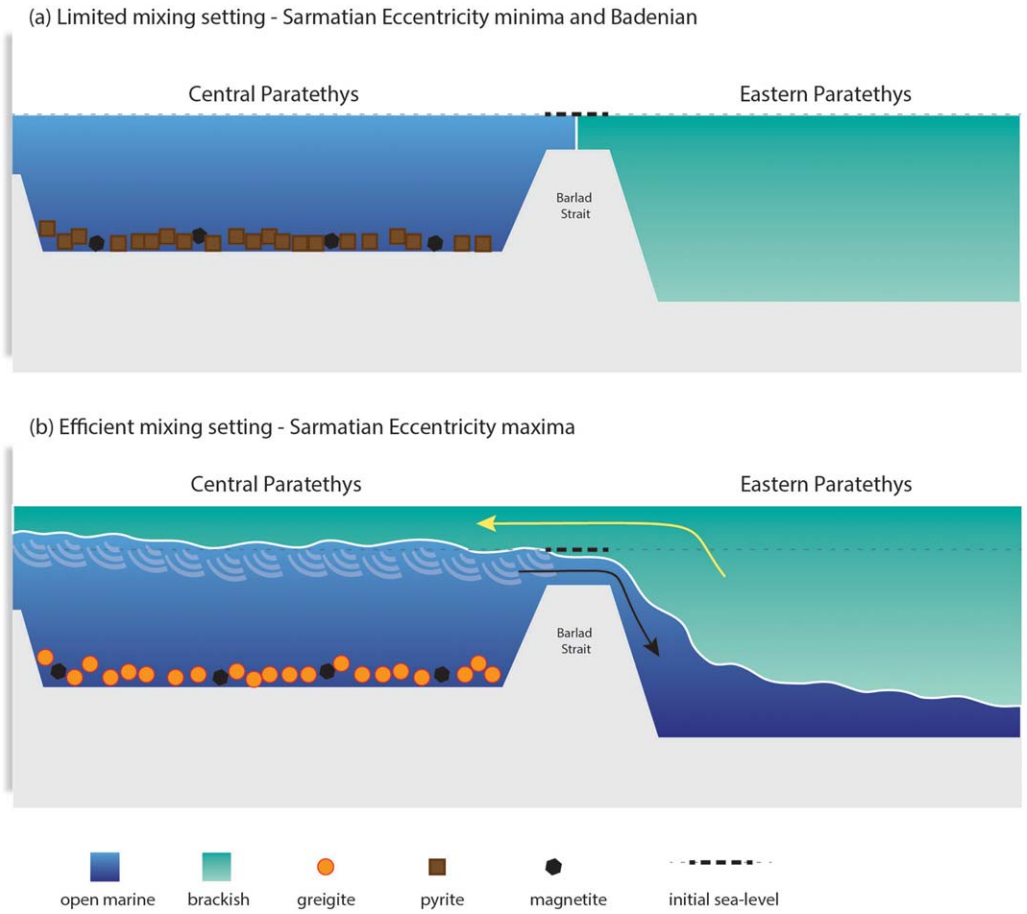

Figure 7. Conceptual model of greigite formation in the Tisa section. (a) During the low magnetic Sarmatian units with eccentricity minima and the Badenian. In a marine setting or a periodical high-salinity settings, the sulfate concentration in the water column in Central Paratethys is high enough for complete pyritization. (b) During the high magnetic Sarmatian units with eccentricity maxima. Fresher and lighter water from the Eastern Paratethys flows into the Central Paratethys (indicated by the yellow arrow from the east to the west), lowering the salinity in the Central Paratethys. Reduced sulfate availability results in insufficient HS^- compared to Fe^{2+}. Pyritization is arrested and therefore greigite is preserved in the sediments.

Paratethys to the Central Paratethys. This will reduce the sulfate availability in the sedimentary environment, which limits the production of HS^-. Therefore, local starvation of sulfide will lead to incomplete pyritization and results in the preservation of greigite. During the eccentricity minima, on the contrary, an increasing Antarctic ice sheet size lowers the sea level. Reduced infilling of fresh water leads to water conditions with higher salinity and higher sulfate availability. This facilitates sulfate reduction, and thus sufficient HS^- over Fe^{2+} is available to form pyrite. The greigite-pyrite indicator is probably more sensitive to detect (small) changes in salinity than faunal assemblages, because the 100 kyr variations are not clearly expressed in the fossil record of Tisa [*Palcu et al*., 2015].

Although this model is deemed plausible, presently we cannot exclude other factors which may also play an important role. For example, *Nie et al*. [2017] includes atmospheric CO_2 concentration as a possible cause for the eccentricity cycles in East Asian summer monsoon in the Miocene. To disentangle the effects of these factors, independent proxies for atmospheric CO_2 concentration are needed. Our current results cannot further distinguish between these factors.

6. Conclusions

Standard rock magnetic and XRF studies suggest that the greigite layers in the Tisa section correlate neither with terrigenous input nor with within-basin biogenic production. We tentatively link the periodical greigite occurrence to the 100 kyr eccentricity cycles. The greigite layers are formed due to insufficient sulfate when

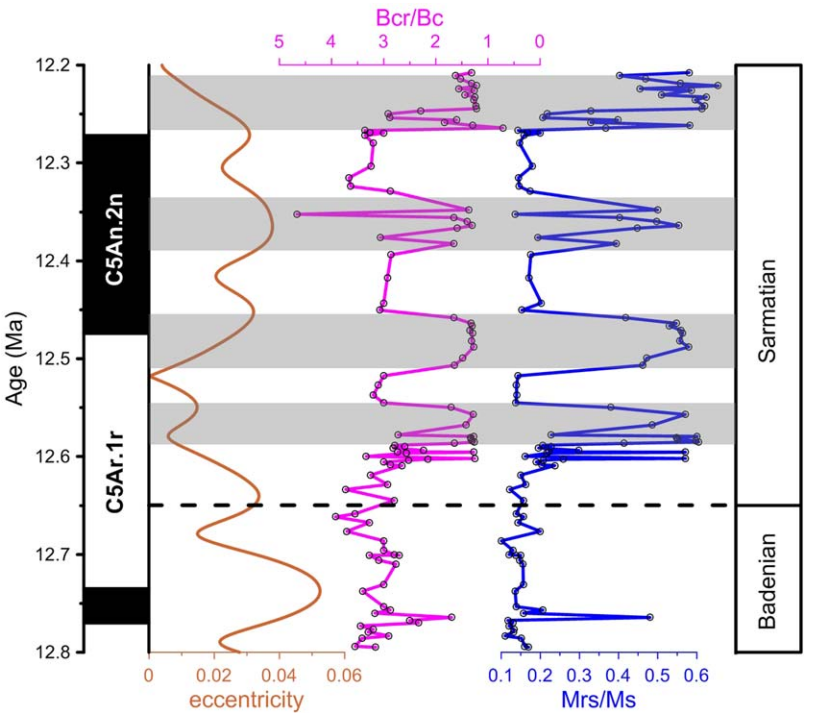

Figure 8. Comparison of magnetic mineral alternations in Tisa with eccentricity. Magnetostratigraphy from *Palcu et al*. [2015] is plotted on the left. The dashed line shows the Badenian-Sarmatian boundary. The greigite-rich layers (indicated by gray bars) broadly coincide with eccentricity maxima, which implies a possible orbital driver of the envisaged fresh water plumes to the Central Paratethys from the Eastern Paratethys.

freshwater flowing into the basin reduced the salinity. During the marine Badenian, abundant sulfate supply enables a surplus of HS^- over Fe^{2+} and thus production of pyrite. During the Sarmatian, periodic plumes through the Barlad Gateway bring fresh water from the Eastern Paratethys. During eccentricity maxima, infilling freshwater into the Central Paratethys reduced the sulfate availability and limits the HS^- production. Insufficient HS^- therefore leads to preservation of greigite in the sediments. We tentatively relate the eccentricity cycles to Antarctic ice sheet driving. Yet our results do not exclude other possible mechanisms such as CO_2 concentration being the driver. Overall, our results suggest the potential of greigite as an indicator of salinity changes, at least during transitions from marine to lacustrine conditions in the Central Paratethys.

Early diagenetic greigite in the Tisa section documents a quasi-primary paleomagnetic signal which yields reliable magnetostratigraphy [*Palcu et al*., 2015]. Since many magnetostratigraphic data in the Paratethys realm come from greigite-bearing sediments, we suggest that a detailed investigation into greigite's origin be performed on a case-by-case basis. Greigite that forms during the early diagenesis, as shown in this study, can yield reliable ages and paleoenvironmental implications. A detailed investigation of the greigite formation mechanism, a good correlation with the global geomagnetic polarity time scale, and positive paleomagnetic field tests can constrain the reliability of paleomagnetic dating.

Acknowledgments
This work was financially supported by the Netherlands Geosciences Foundation (ALW) with support from the Netherlands Organization for Scientific Research (NWO) through the VICI grant of Wout Krijgsman. We thank Maxim Krasnoperov for his instruction on XRF, Zhongshan Shen and Shuangchi Liu from Beijing for low-temperature measurements on MPMS, Frits Hilgen, Chunxia Zhang, Chenglong Deng, and Bill Ruddiman for insightful discussions. We are grateful to Joshua Feinberg for his efficient editorial handling and to Liao Chang and an anonymous reviewer for their suggestions that significantly improved the manuscript. Suzhen Liu acknowledges further the NSFC grants 41574061 and the CPSF-CAS Joint Foundation for Excellent Postdoctoral Fellows. The original data to produce the figures and supplementary figures in this paper can be found in the Supplementary Information or obtained by contacting the corresponding author (s.liu@uu.nl).

References

Aben, F. M., M. J. Dekkers, R. R. Bakker, D. J. J. van Hinsbergen, W. J. Zachariasse, G. W. Tate, N. McQuarrie, R. Harris, and B. Duffy (2014), Untangling inconsistent magnetic polarity records through an integrated rock magnetic analysis: A case study on Neogene sections in East Timor, *Geochem. Geophys. Geosyst.*, *15*, 2531–2554, doi:10.1002/2014GC005294.

Babinszki, E., E. Marton, P. Marton, and L. F. Kiss (2007), Widespread occurrence of greigite in the sediments of Lake Pannon: Implications for environment and magnetostratigraphy, *Palaeogeogr. Palaeoclimatol. Palaeoecol.*, *252*, 626–636.

Beaufort, L. (1994), Climatic importance of the modulation of the 100-kyr cycle inferred from 16 m.y. long Miocene records, *Paleoceanography*, *9*, 821–834.

Berner, R. A. (1984), Sedimentary pyrite formation: An update, *Geochim. Cosmochim. Acta*, *48*, 605–615.

Blanchet, C. L., N. Thouveny, and L. Vidal (2009), Formation and preservation of greigite (Fe_3S_4) in sediments from the Santa Barbara Basin: Implications for paleoenvironmental changes during the past 35 ka, *Paleoceanography*, *24*, 15.

Chang, L., I. Vasiliev, C. van Baak, W. Krijgsman, M. J. Dekkers, A. P. Roberts, J. D. F. Gerald, A. van Hoesel, and M. Winklhofer (2014), Identification and environmental interpretation of diagenetic and biogenic greigite in sediments: A lesson from the Messinian Black Sea, *Geochem. Geophys. Geosyst.*, *15*, 3612–3627, doi:10.1002/2014GC005411.

Chang, L., A. P. Roberts, D. Heslop, A. Hayashida, J. H. Li, X. Zhao, W. Tian, and Q. H. Huang (2016), Widespread occurrence of silicate-hosted magnetic mineral inclusions in marine sediments and their contribution to paleomagnetic recording, *J. Geophys. Res. Solid Earth*, *121*, 8415–8431, doi:10.1002/2016JB013109.

Chen, J., Z. An, and J. Head (1999), Variation of Rb/Sr ratios in the loess-paleosol sequences of central China during the last 130,000 years and their implications for monsoon paleoclimatology, *Quat. Res.*, *51*, 215–219.

Day, R., M. Fuller, and V. A. Schmidt (1977), Hysteresis properties of titanomagnetites—Grain-size and compositional dependence, *Phys. Earth Planet. Inter.*, *13*, 260–267.

Dekkers, M. J., H. F. Passier, and M. A. A. Schoonen (2000), Magnetic properties of hydrothermally synthesized greigite (Fe_3S_4)—II. High- and low-temperature characteristics, *Geophys. J. Int.*, *141*, 809–819.

de Leeuw, A., S. Filipescu, L. Matenco, W. Krijgsman, K. Kuiper, and M. Stoica (2013), Paleomagnetic and chronostratigraphic constraints on the Middle to Late Miocene evolution of the Transylvanian Basin (Romania): Implications for Central Paratethys stratigraphy and emplacement of the Tisza-Dacia plate, *Global Planet. Change*, *103*, 82–98.

Dunlop, D. J. (2002), Theory and application of the Day plot (*Mrs*/*Ms* versus *Hcr*/*Hc*) 1. Theoretical curves and tests using titanomagnetite data, *J. Geophys. Res.*, *107*(B3), doi:10.1029/2001JB000486.

Fu, Y. Z., T. von Dobeneck, C. Franke, D. Heslop, and S. Kasten (2008), Rock magnetic identification and geochemical process models of greigite formation in Quaternary marine sediments from the Gulf of Mexico (IODP Hole U1319A), *Earth Planet. Sci. Lett.*, *275*, 233–245.

Harzhauser, M., and W. E. Piller (2007), Benchmark data of a changing sea-Palaeogeography, palaeobiogeography and events in the Central Paratethys during the Miocene, *Palaeogeogr. Palaeoclimatol. Palaeoecol.*, *253*, 8–31.

Hays, J. D., J. Imbrie, and N. J. Shackleton (1976), Variations in the Earth's orbit: Pacemaker of the Ice Ages, *Science*, *194*, 1121–1132.

Heslop, D., and A. P. Roberts (2012), Estimation of significance levels and confidence intervals for first-order reversal curve distributions, *Geochem. Geophys. Geosyst.*, *13*, Q12Z40, doi:10.1029/2012GC004115.

Hsü, K. J., and F. Giovanoli (1979), Messinian event in the Black Sea, *Palaeogeogr. Palaeoclimatol. Palaeoecol.*, *29*, 75–93.

Imbrie, J., et al. (1993), On the structure and origin of major glaciation cycles 2. The 100,000-year cycle, *Paleoceanography*, *8*, 699–735.

Jaccard, S. L., G. H. Haug, D. M. Sigman, T. F. Pedersen, H. R. Thierstein, and U. Röhl (2005), Glacial/interglacial changes in Subarctic North Pacific stratification, *Science*, *308*, 1003–1006.

Jiang, W. T., C. S. Horng, A. P. Roberts, and D. R. Peacor (2001), Contradictory magnetic polarities in sediments and variable timing of neoformation of authigenic greigite, *Earth Planet. Sci. Lett.*, *193*, 1–12.

Kao, S. J., C. S. Horng, A. P. Roberts, and K. K. Liu (2004), Carbon-sulfur-iron relationships in sedimentary rocks from southwestern Taiwan: Influence of geochemical environment on greigite and pyrrhotite formation, *Chem. Geol.*, *203*, 153–168.

Karami, M. P., A. de Leeuw, W. Krijgsman, P. T. Meijer, and M. J. R. Wortel (2011), The role of gateways in the evolution of temperature and salinity of semi-enclosed basins: An oceanic box model for the Miocene Mediterranean Sea and Paratethys, *Global Planet. Change*, *79*, 73–88.

Krijgsman, W., M. Stoica, I. Vasiliev, and V. V. Popov (2010), Rise and fall of the Paratethys Sea during the Messinian Salinity Crisis, *Earth Planet. Sci. Lett.*, *290*, 183–191.

Król, E., and M. Jeleńska (1999), The local magnetostratigraphic scale for the supra-evaporitic Miocene deposits in the northern part of Carpathian Foredeep and its stratigraphic implications (drill-core Jamnica S-119), *Geol. Quart.*, *43*, 509–518.

Kukla, G., F. Heller, X. M. Liu, T. C. Xu, T. S. Liu, and Z. S. An (1988), Pleistocene climates in China dated by magnetic-susceptibility, *Geology*, *16*, 811–814.

Laskar, J., P. Robutel, F. Joutel, M. Gastineau, A. C. M. Correia, and B. Levrard (2004), A long-term numerical solution for the insolation quantities of the Earth, *Astron. Astrophys.*, *428*, 261–285.

Laskarev, V. (1924), Sur les equivalents du Sarmatien superieur en Serbie, in *Receuil de traveaux offert á M. Jovan Cvijic par ses amis et collaborateurs*, edited by P. Vujević, pp. 73–85, Drzhavna Shtamparija, Beograd.

Mullender, T. A. T., A. J. van Velzen, and M. J. Dekkers (1993), Continuous drift correction and separate identification of ferrimagnetic and paramagnetic contributions in thermomagnetic runs, *Geophys. J. Int.*, *114*, 663–672.

Nie, J., C. Garzione, Q. Su, Q. Liu, R. Zhang, D. Heslop, C. Necula, S. Zhang, Y. Song, and Z. Luo (2017), Dominant 100,000-year precipitation cyclicity in a late Miocene lake from northeast Tibet, *Sci. Adv.*, *3*, e1600762.

Oda, H., and M. Torii (2004), Sea-level change and remagnetization of continental shelf sediments off New Jersey (ODP Leg 174A): Magnetite and greigite diagenesis, *Geophys. J. Int.*, *156*, 443–458.

Palcu, D. V., M. Tulbure, M. Bartol, T. J. Kouwenhoven, and W. Krijgsman (2015), The Badenian-Sarmatian Extinction Event in the Carpathian foredeep basin of Romania: Paleogeographic changes in the Paratethys domain, *Global Planet. Change*, *133*, 346–358.

Passier, H. F., G. J. de Lange, and M. J. Dekkers (2001), Magnetic properties and geochemistry of the active oxidation front and the youngest sapropel in the eastern Mediterranean Sea, *Geophys. J. Int.*, *145*, 604–614.

Ramstein, G., F. Fluteau, J. Besse, and S. Joussaume (1997), Effect of orogeny, plate motion and land sea distribution on Eurasian climate change over the past 30 million years, *Nature*, *386*, 788–795.

Raymo, M. E. (1994), The initiation of Northern Hemisphere glaciation, *Ann. Rev. Earth Planet. Sci.*, *22*, 353–383.

Reynolds, R., and J. G. Rosenbaum (2005), Magnetic mineralogy of sediments in Bear Lake and its watershed, Utah, Idaho, and Wyoming: Support for paleoenvironmental and paleomagnetic interpretations, in *Magnetic Properties of Sediments in Cores BL96–1, −2, and −3 From Bear Lake, Utah and Idaho*, edited by J. G. Rosenbaum, *U.S. Geol. Surv. Open File Rep., 2015–1406*, 17 pp.

Reynolds, R. L., J. G. Rosenbaum, N. Mazza, W. Rivers, and F. Luiszer (1998), Sediment magnetic data (83 to 18 m depth) and XRF geochemical data (83 to 32 m depth) from lacustrine sediment in core OL-92 from Owens Lake, California, in The Last Interglaciation at Owens Lake, California: Core OL-92, edited by J. L. Bischoff, U.S. Geol. Surv. Open File Rep., 98–132, pp. 99–119.

Roberts, A. P., and R. Weaver (2005), Multiple mechanisms of remagnetization involving sedimentary greigite (Fe_3S_4), *Earth Planet. Sci. Lett.*, *231*, 263–277.

Roberts, A. P., Q. S. Liu, C. J. Rowan, L. Chang, C. Carvallo, J. Torrent, and C. S. Horng (2006), Characterization of hematite (α-Fe_2O_3), goethite (α-FeOOH), greigite (Fe_3S_4), and pyrrhotite (Fe_7S_8) using first-order reversal curve diagrams, *J. Geophys. Res.*, *111*, B12S35, doi:10.1029/2006JB004715.

Roberts, A. P., L. Chang, C. J. Rowan, C. S. Horng, and F. Florindo (2011), Magnetic properties of sedimentary greigite (Fe_3S_4): An update, *Rev. Geophys.*, *49*, RG1002, doi:10.1029/2010RG000336.

Rögl, F. (1999), Mediterranean and Paratethys: Facts and hypotheses of an Oligocene to Miocene paleogeography (short overview), *Geol. Carpath.*, *50*, 339–349.

Rowan, C. J., and A. P. Roberts (2006), Magnetite dissolution, diachronous greigite formation, and secondary magnetizations from pyrite oxidation: Unravelling complex magnetizations in Neogene marine sediments from New Zealand, *Earth Planet. Sci. Lett.*, *241*, 119–137.

Ruddiman, W. F. (2014), *Earth's Climate: Past and Future*, 171 pp., Freeman, New York.

Sagnotti, L., A. Cascella, N. Ciaranfi, P. Macri, P. Maiorano, M. Marino, and J. Taddeucci (2010), Rock magnetism and palaeomagnetism of the Montalbano Jonico section (Italy): Evidence for late diagenetic growth of greigite and implications for magnetostratigraphy, *Geophys. J. Int.*, *180*, 1049–1066.

Sant, K., A. de Leeuw, L. Chang, G. Czapowski, A. Gąsiewicz, and W. Krijgsman (2015), Paleomagnetic analyses on Badenian-Sarmatian drill cores from the North Carpathian Foredeep (Middle Miocene, Poland), *Biuletyn Pánstwowego Instytutu Geologicznego*, *461*, 179–192.

Schulz, H. M., A. Bechtel, and R. F. Sachsenhofer (2005), The birth of the Paratethys during the Early Oligocene: From Tethys to an ancient Black Sea analogue? *Global Planet. Change*, *49*, 163–176.

van Baak, C. G. C., I. Vasiliev, D. V. Palcu, M. J. Dekkers, and W. Krijgsman (2016), A greigite-based magnetostratigraphic time frame for the Late Miocene to recent DSDP Leg 42B cores from the Black Sea, *Front. Earth Sci.*, *4*, 60.

Vasiliev, I., W. Krijgsman, C. G. Langereis, C. E. Panaiotu, L. Maţenco, and G. Bertotti (2004), Towards an astrochronological framework for the Eastern Paratethys Mio-Pliocene sedimentary sequences of the Focşani basin (Romania), *Earth Planet. Sci. Lett.*, *227*, 231–247.

Vasiliev, I., W. Krijgsman, M. Stoica, and C. G. Langereis (2005), Mio-Pliocene magnetostratigraphy in the southern Carpathian foredeep and Mediterranean-Paratethys correlations, *Terra Nova*, *17*, 376–384.

Vasiliev, I., M. J. Dekkers, W. Krijgsman, C. Franke, C. G. Langereis, and T. A. T. Mullender (2007), Early diagenetic greigite as a recorder of the palaeomagnetic signal in Miocene-Pliocene sedimentary rocks of the Carpathian foredeep (Romania), *Geophys. J. Int.*, *171*, 613–629.

Vasiliev, I., C. Franke, J. D. Meeldijk, M. J. Dekkers, C. G. Langereis, and W. Krijgsman (2008), Putative greigite magnetofossils from the Pliocene epoch, *Nat. Geosci.*, *1*, 782–786.